REVISTA INVESTIGACION OPERACIONAL
https://doi.org/10.5281/zenodo.23302386 **VOL. 48, NO.1, 102-117, 2027**

ENVIRONMENTAL MONITORING AND FINITE-STATE SUPERVISORY CLIMATE CONTROL IN AN EXPERIMENTAL GREENHOUSE

Secundino Marrero Ramírez[1], Carlos Pacheco Mena, Marco León Segovia, Ángel León Segovia
Facultad de Ciencias de la Ingeniería y Aplicada, Universidad Técnica de Cotopaxi, Latacunga, Ecuador.

ABSTRACT

An experimental 50 m² shaded greenhouse was instrumented with type-K thermocouples, eight FC-28 probes, an ultrasonic level sensor and a power analyser under a PLC and a SCADA system, and supplied by a 1500 Wp photovoltaic array with a 500 Ah battery bank and grid transfer. This paper reports what that platform measures and formalises the control policy it executes. The humidity channel is substrate moisture, not atmospheric relative humidity: the FC-28 is a soil hygrometer, the interface sets one moisture target per crop row, and the loop it closes is irrigation. No atmospheric-humidity instrument is documented, so no air-humidity measurement or control is claimed. The temperature controller is a four-mode finite-state supervisory policy that escalates window opening, forced extraction and misting while the indoor temperature stays above a single configurable reference; the deployed flowchart records neither a release margin nor a humidity interlock, both proposed here for a future implementation. The identified outdoor-to-indoor temperature model is retained with an 88 % in-sample fit, no held-out validation and a time unit that the available data do not fix; the nominal air-exchange time V/Q = 128.6 s is a ventilation quantity, not an identified thermal constant. Over seven days the analyser recorded an average load of 7 kWh per day; usable storage energy is undetermined without the bus voltage, depth of discharge and conversion efficiency, so no autonomy is claimed. A 90.0 % germination rate is reported descriptively, without a baseline cycle and therefore without causal attribution.

KEYWORDS: greenhouse automation; supervisory control; finite-state policy; system identification; substrate moisture; photovoltaic microgrid.

MSC: 93C95, 90B50, 68M14.

RESUMEN

Un invernadero experimental sombreado de 50 m² se instrumentó con termopares tipo K, ocho sondas FC-28, un sensor ultrasónico de nivel y un analizador de red bajo un PLC y un sistema SCADA, y se alimenta de un generador fotovoltaico de 1500 Wp con un banco de 500 Ah y conmutación a la red. Este trabajo reporta qué mide esa plataforma y formaliza la política de control que ejecuta. El canal de humedad es humedad de sustrato y no humedad relativa del aire: el FC-28 es un higrómetro de suelo, la interfaz fija una consigna por hilera y el lazo que cierra es el de riego. No consta ningún instrumento de humedad atmosférica, de modo que no se afirma medición ni control de la humedad del aire. El control de temperatura es una política supervisora de estados finitos de cuatro modos que escalona ventanas, extracción forzada y nebulización mientras la temperatura interior supera una única referencia configurable; el diagrama desplegado no registra margen de liberación ni enclavamiento de humedad, ambos propuestos aquí para una implementación futura. El modelo identificado entre temperatura exterior e interior se conserva con un ajuste del 88 % en la propia muestra, sin validación independiente y con una unidad de tiempo que el registro no fija; el tiempo nominal de renovación de aire V/Q = 128,6 s es una magnitud de ventilación y no una constante térmica identificada. En siete días el analizador registró una carga media de 7 kWh diarios; la energía utilizable del acumulador queda indeterminada sin la tensión de bus, la profundidad de descarga y el rendimiento de conversión, por lo que no se afirma autonomía. Se reporta una germinación del 90,0 % de forma descriptiva, sin ciclo de referencia y por tanto sin atribución causal.

PALABRAS CLAVE: automatización de invernaderos; control supervisor; política de estados finitos; identificación de sistemas; humedad de sustrato; microrred fotovoltaica.

1. INTRODUCTION

Greenhouse production allows early harvests, higher quality and yield, off-season crops, savings in water and fertiliser and better control of pests and diseases, at the cost of a high initial investment, significant operating costs and the need

[1] Corresponding author: secundino.marrero@utc.edu.ec

for qualified personnel [9, 16]. Control technology is what turns those advantages into practice: the works of Alarcón et al. [1], Mamani et al. [15], Tangarife et al. [25] and Marrero et al. [17] identify indoor temperature, humidity and CO_2 concentration as the variables to be regulated as a function of solar radiation, and report heating, ventilation, humidification, thermal screens, CO_2 dosing and supplementary lighting as the usual means of acting on them.

Ventilation deserves separate mention because it is the actuator used here. Estimating the ventilation rate yields an average global air exchange across all openings, and whether the windows dominate that exchange is still under study [3]. Numerical methods and computational fluid dynamics have deepened the analysis [8, 28], and multivariable, predictive and fuzzy schemes have been applied to greenhouse climate [5, 7], with Trejo and Lorenzo [27] reviewing the artificial-intelligence techniques used for modelling and control in this domain. Climate-smart agriculture adds a further motive: with 40 % of the world's agricultural land degraded, precision management is one of the few levers available, and its adoption is limited by cost rather than by technique [11, 14].

This paper reports an instrumented experimental greenhouse and does two things with it. First, it states precisely which physical quantities the installed instrumentation measures: the humidity channel is substrate moisture and not atmospheric relative humidity, and that distinction changes which loop is being closed and which claims the platform can support. Second, it formalises the temperature controller actually deployed as a finite-state supervisory policy, separating what the engineering documentation fixes from what it leaves open. The identified thermal model, the ventilation sizing and the photovoltaic subsystem are treated with the same criterion: a quantity is reported when the available data determine it, and its absence is declared when they do not.

2. MATERIALS AND METHODS

The work combines system identification, modelling and field experimentation. An experimental shaded greenhouse of 50 m² was used for seedling production, with three irrigation rows holding the seed trays, located on the Salache campus of the Universidad Técnica de Cotopaxi at an altitude of 2750 m. The shaded type was chosen for its greater capacity to control climatic factors, which is the criterion Montero, Stanghellini and Castilla [19] apply to greenhouse design for mild-winter climates. Off-on controllers were adopted for both regulated variables in order to keep the control algorithms simple.

2.1 Photovoltaic microgrid

The greenhouse is supplied by the microgrid of Figure 1: a 1500 Wp photovoltaic array, a charge regulator, a battery bank rated at 500 Ah, an inverter and an automatic transfer system that also accepts the ELEPCO S.A. utility supply. The average solar irradiance of the site is 552.98 $W \cdot m^{-2}$. Two loads hang from the transfer system, the greenhouse and the adjacent Andean grains laboratory. The topology matters for what can later be claimed about energy: the laboratory is a parallel load on the same transfer system rather than the recipient of an exported surplus, and the presence of the transfer switch means that the load may be served from the grid whenever the photovoltaic subsystem does not cover it.

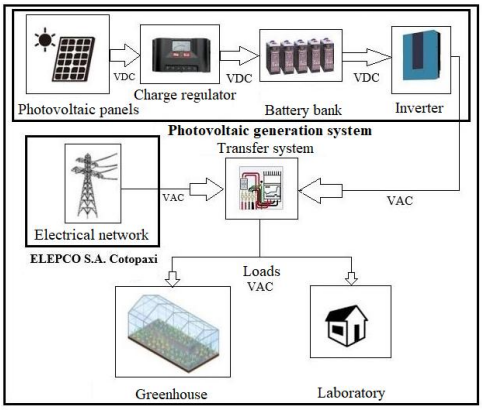


Figure 1. Photovoltaic microgrid. The utility supply enters through the automatic transfer system, and the greenhouse and the laboratory are parallel loads on it.

2.2 Instrumentation and the quantities actually measured

Indoor air temperature is measured with type-K thermocouples (TERMO-K-12). Humidity is measured with eight FC-28 hygrometers distributed in the row trays [4, 18]. The FC-28 is a resistive probe with adjustable sensitivity and digital and analogue outputs, with a response time of the order of seconds; the signal reaches the PLC through an Arduino Mega board. According to the engineering documentation of the installation, the probes were adjusted against an HM 445 digital meter reported with ±5 % accuracy; the calibration curve and the resulting measurement uncertainty of the FC-28 channel are not available, so that ±5 % is the figure of the reference instrument and not an accuracy of the FC-28.

The general configuration of the SCADA system is shown in Figure 2. Two process channels reach the S7-1200 PLC — temperature and humidity — and a third, energy, is served by the Sentron PAC 3200 analyser, all of them carried over a data channel of 5 Mbps — an architecture of the same family as the fieldbus-based greenhouse control of Zhang et al. [29]. The single humidity channel is the FC-28 signal.

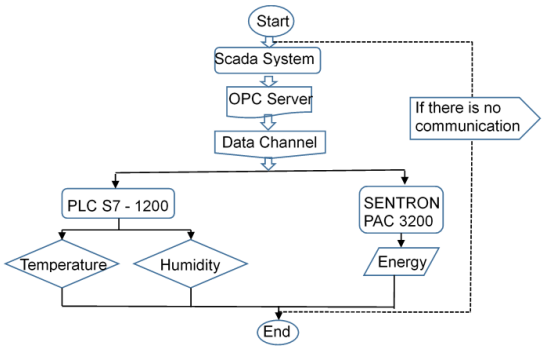


Figure 2. SCADA system configuration. The PLC serves one temperature channel and one humidity channel; the humidity channel is the substrate-moisture signal.

The FC-28 is a soil hygrometer. It measures the electrical conductivity between two electrodes buried in the substrate, and what that conductivity tracks is the substrate-moisture level indicated by the FC-28, not the water vapour content of the air above it. Two distinct variables are therefore used throughout this paper: M_{soil}, which the eight FC-28 probes report, and atmospheric relative humidity $\mathrm{RH}_{\mathrm{air}}$, which no instrument in the installation measures. M_{soil} denotes the FC-28 substrate-moisture index on the controller's percentage scale; the notation deliberately avoids the symbol conventionally reserved for volumetric water content. The FC-28 output is interpreted here as a substrate-moisture index on the controller's percentage scale, not as volumetric water content: there is no calibration curve, no conversion to volumetric or gravimetric water content and no traceable physical unit for this channel. Table 1 lists the instrumentation of the installation and, in the last column, what its documentation does not fix.

Quantity	Instrument	Loop served	Fixed by the documentation	Not documented
Indoor air temperature	Type-K thermocouple (TERMO-K-12)	Temperature escalation	Model designation; signal to the S7-1200 PLC	Number of probes, placement height, range, accuracy
Substrate-moisture index, M_{soil} (%)	FC-28 resistive soil hygrometer (× 8), via Arduino Mega	Irrigation	Eight units in the row trays; response time of the order of seconds; adjustment against an HM 445 reference meter reported with ±5 % accuracy	Range; accuracy of the FC-28 channel after adjustment; calibration curve; residuals; conversion from the percentage scale to volumetric or gravimetric water content
Atmospheric relative humidity, $\mathrm{RH}_{\mathrm{air}}$	None documented	—	—	The quantity itself: no atmospheric-humidity transmitter appears in the equipment list, in the SCADA configuration or in the control schematic
Irrigation tank level	Ultrasonic sensor	Daily water consumption	Presence in the control schematic and its wiring to the PLC	Manufacturer, model, range, accuracy
Electrical energy	Sentron PAC 3200 power analyser	Energy monitoring	One energy channel reported to the SCADA system	Separation between photovoltaic generation, battery flow and grid import
Outdoor air temperature	Not identified	Input of the identified model	Its use as the model input	Instrument, placement, shielding, range, accuracy

Table 1. Instrumentation of the installation. The third row is the key point: the installation has no atmospheric-humidity sensor, so relative humidity of the air is neither measured nor controlled by the deployed system.

2.3 Reference climate models

Multivariable models of the greenhouse climate are of interest as a reference frame even when the deployed controller does not use them. The models of Salazar, López and Sánchez [23] and Castañeda, Herrera and García [6] are based on the energy balance of the indoor air and of the crop, equations (1) and (2), which collect the heat fluxes q by conduction, convection, radiation, vaporisation, crop radiation and ventilation:

$$q_{\mathrm{conv}} - q_{\mathrm{ven}} = V_{\mathrm{l}}\rho_{\mathrm{l}}c_{\mathrm{p}}\frac{\mathrm{d}T_{\mathrm{i}}}{\mathrm{d}t} \tag{1}$$

$$q_{\mathrm{abs}} + q_{\mathrm{c,rad}} - q_{\mathrm{c,conv}} - q_{\mathrm{c,evap}} = \mathrm{LAI}\delta_{\mathrm{c}}\rho_{\mathrm{c}}c_{\mathrm{c}}\frac{\mathrm{d}T_{\mathrm{c}}}{\mathrm{d}t} \tag{2}$$

The work of Salazar et al. [22] adds the indoor humidity balance, equation (3), a differential equation for the absolute humidity of the air X_{a} driven by crop transpiration E, condensation in heat exchange C and the greenhouse height h:

$$\frac{\mathrm{d}X_{\mathrm{a}}}{\mathrm{d}t} = \frac{1}{h}(E - C) \tag{3}$$

Symbols: q_{conv} convective heat flow; q_{ven} ventilation heat flow; q_{abs} absorbed heat flow; $q_{\mathrm{c,rad}}$ radiative heat flow in the plant; $q_{\mathrm{c,conv}}$ convective heat flow in the plant; $q_{\mathrm{c,evap}}$ heat transferred by evaporation; V_{l} ratio of air volume to floor area; ρ_{l} air density; c_{p} specific heat of air at constant pressure; c_{c} specific heat of the leaf; δ_{c} leaf density; LAI leaf area index; T_{i} indoor air temperature; T_{c} crop temperature.

Equation (3) is stated here for completeness and as the natural target of a future atmospheric-humidity loop. It is not instantiated in this work, because X_{a} requires a measurement of the water vapour content of the indoor air that the installation does not provide.

3. THE DEPLOYED SUPERVISORY CONTROL POLICY

3.1 Irrigation loop on substrate moisture

The humidity algorithm of Figure 3 admits manual and automatic operation. In automatic mode a set point is entered as a percentage and compared with the FC-28 reading; when the measured value falls below the set point the pump is started and the row is irrigated. The band entered in the flowchart runs from 40 to 80 %. Both branches of the diagram take their measurement from the same source, labelled Sensor FC-28, and the actuator both branches command is the irrigation pump.

This is an irrigation loop, not a climate loop. It regulates the substrate-moisture level indicated by the FC-28 in each row by adding water to the substrate, and it has no path by which it could regulate the water vapour content of the greenhouse air. The human-machine interface (Figure 4b) makes the same point from the operator's side: it exposes one set point and one measured value per row, for three rows, which is meaningful for substrate moisture — the rows can legitimately be at different moisture levels, and a row that is not in use need not be irrigated — and is not meaningful for atmospheric relative humidity, which is a property of the shared air volume.

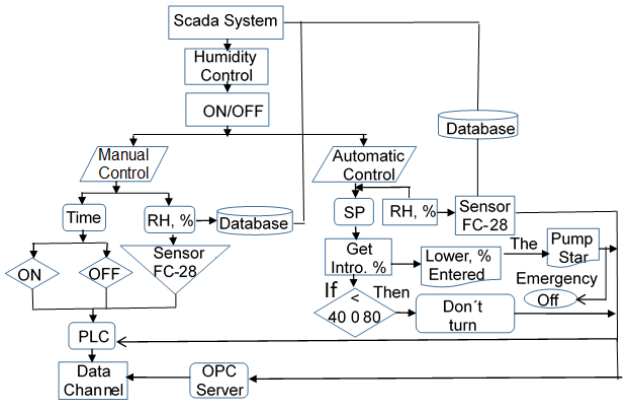
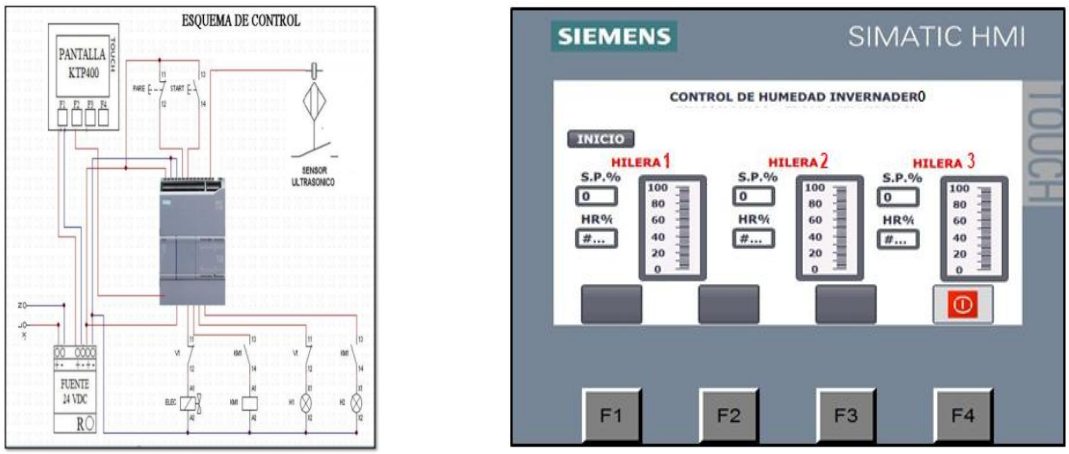


Figure 3. Substrate-moisture control diagram. The only sensor in the loop is the FC-28 and the only actuator is the irrigation pump; the percentage labelled RH in the original diagram is the substrate-moisture reading.



(a) (b)

Figure 4. Control schematic with the ultrasonic level sensor of the irrigation tank (a) and interface for substrate-moisture control by row (b). The interface exposes one set point and one measured value for each of the three rows.

3.2 Temperature escalation

The temperature algorithm of Figure 5 is organised in three stages. The indoor temperature is compared with a reference T_{ref}. While the temperature stays above the reference the controller escalates: stage 1 opens the windows, stage 2 adds the forced-air extractor and stage 3 adds the misting system, which is driven from the irrigation circuit and cools by evaporation, the mechanism Alves et al. [2] characterise for evaporative cooling in greenhouses. A time rule closes the windows after 18:00, since night and early-morning temperatures are generally below the target; the two synchronised motors that drive them place this actuator in the same class as the roll-up screen positioning studied by Guoxiang et al. [10].

Read as a control policy, the flowchart fixes less than a narrative description suggests, and the difference is worth stating explicitly because it determines what can be reproduced. Every decision node in Figure 5 tests the same condition, temperature against a single reference T_{ref}; there are not three distinct thresholds but one, re-evaluated after each stage has been allowed to act. Escalation is therefore driven by the persistence of the same condition, not by crossing successive set points. No release margin appears anywhere in the diagram: when the test succeeds the prescribed action is to maintain the previous condition, so the deployed logic contains no de-escalation transition other than the 18:00 window rule. And no humidity condition gates the misting stage: stage 3 is entered on the temperature test alone.

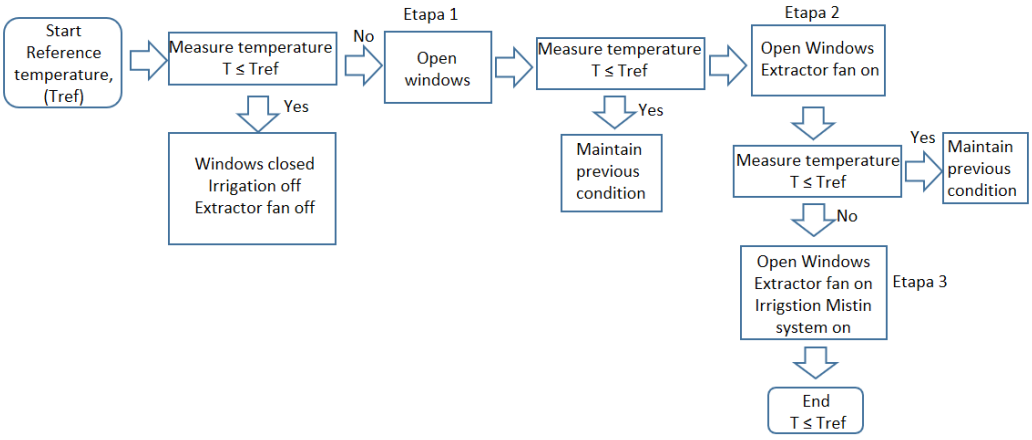


Figure 5. Deployed temperature control flowchart. Every decision node tests the same condition against a single reference temperature, and the escalation is driven by the persistence of that condition rather than by successive thresholds.

The policy is stated as a four-mode finite-state supervisory machine in Table 2, with the guards written as the flowchart writes them. Empty entries are the places where the deployed configuration fixes no value.

Mode	Active actuators	Activation guard	Release guard	Interlock
S0	None: windows closed, extractor off, misting off	$T \leq T_{\mathrm{ref}}$ (initial mode)	—	—
S1	Windows open	$T > T_{\mathrm{ref}}$	Not documented	—
S2	Windows + forced-air extractor	$T > T_{\mathrm{ref}}$ persists after S1	Not documented	—
S3	Windows + extractor + misting	$T > T_{\mathrm{ref}}$ persists after S2	Not documented	None deployed

Table 2. Supervisory control policy as deployed, read from Figure 5. A single reference temperature $\mathrm{T_{ref}}$ governs all four guards; the release and interlock columns show what the deployed configuration does not fix. A time rule closes the windows after 18:00.

3.3 What the deployed configuration fixes and what it does not

The escalation structure is reproducible: the modes, the actuators active in each of them, the order of escalation and the condition that drives it are all determined by Figure 5. The numerical content is not. The reference T_{ref} is configurable from the interface, which also accepts a minimum and a maximum temperature and a misting time, and no deployed value of any of them was preserved. The one numerical statement in the text — that automatic control operates from 20 °C — describes the lower end of the configurable range rather than a transition threshold, and the values 28 °C, 25 °C and 31 °C that appear later belong to a simulation of the on-off extractor loop and cannot be identified with the escalation stages. What this paper delivers is therefore a reproducible formal structure, not a fully reproducible deployed policy.

Two elements that a supervisory policy of this kind normally carries are absent from the deployed logic and are proposed here for a future implementation, clearly separated from what was executed. The first is a release margin: making the release guard of each mode strictly lower than its activation guard prevents the actuators from chattering around a single set point, which the present logic avoids only by never de-escalating. The second is an interlock on the misting stage. Misting cools by evaporation and therefore raises the humidity of the air, and the operationally relevant guard would prevent it near saturation; that guard requires an atmospheric-humidity measurement the installation does not have. A substrate-moisture interlock is the only variant the deployed sensing could evaluate, and it protects a different quantity — misting is fed from the irrigation circuit and wets the substrate as well — so it is not a substitute. Neither element should be read as part of the controller that was operated.

3.4 Why a static ranking is not the right abstraction

It is tempting to treat the three actuators as competing alternatives and to rank them by their attributes. That abstraction does not fit the problem. A ranking presupposes that exactly one of the alternatives is to be chosen, whereas the plant escalates and accumulates: the extractor is meaningful only once the windows are already open, and misting only once forced ventilation has proved insufficient. Any static ordering must therefore either contradict the deployed sequence or reproduce it by construction, and in neither case does it say anything about the control problem. The decision variable is not which actuator is best, but in which mode the system should be at each instant, given its thermal state, the accumulated effect of previous actions and the resources available. That is the formulation a finite-horizon optimal control problem with binary decisions would address, and Section 6 states the measurements it requires.

4. RESULTS

The models of equations (1) to (3) require a number of measurements the installation does not provide, so the dynamics used for control design were obtained by identification. The rest of this section reports, in order, that model and its validation status, the ventilation quantity that has been read as a thermal constant, the temperature and substrate-moisture records, the cycle report and the energy subsystem.

4.1 Identified thermal model and its validation status

The relation between outdoor and indoor air temperature was estimated with the Ident tool of MATLAB from data recorded on days with similar levels of radiation and wind speed, yielding equation (4) with a reported fit of 88 %,

one zero and two poles (Figure 6A). Figure 6B shows the simulated response of the indoor temperature to a step of 22 °C in the outdoor temperature.

$$G(s) = \frac{5s + 4.4}{s^2 + 3.5s + 2.8} \tag{4}$$

The model is internally consistent and is retained. Its zero lies at −0.88 and its poles at −2.26 and −1.24, both real and negative, so the response is stable and overdamped, which is what one expects of a thermal envelope. Its static gain is 4.4/2.8 = 1.57, and that value is confirmed by the figure: a step of 22 °C produces a steady state of 34.57 °C, which is the ordinate the plotted response settles on.

Three properties of the identification are not fixed by the available data, and each limits what the model licenses. The identification data set is described qualitatively — several days of similar radiation and wind — without the number of observations, the sampling interval or the dates, and the single record reproduced in Figure 6A spans about 19 h. No held-out interval is reported, so the 88 % figure is an in-sample fit and not a validation; the criterion MATLAB reported was not preserved, and the tool's default is a normalised root-mean-square fit. The model is accordingly described here as an identified model with an 88 % in-sample fit, and not as a validated model.

The time unit is the third gap, and it is the one with consequences. Taken as plotted, with the abscissa of Figure 6B in seconds, the dominant time constant of equation (4) is 0.81 s and the response settles in about five seconds; a 150 m³ greenhouse does not do that, and the identification record of Figure 6A spans about 19 h. Read instead with the sample index in hours, the same transfer function gives a dominant time constant of 48.5 min, which is the order of magnitude a shaded greenhouse of this size has. The sample time supplied to the identification tool was not preserved, so the discrepancy is reported rather than resolved: the coefficients of equation (4) are preserved, and the time unit remains open.

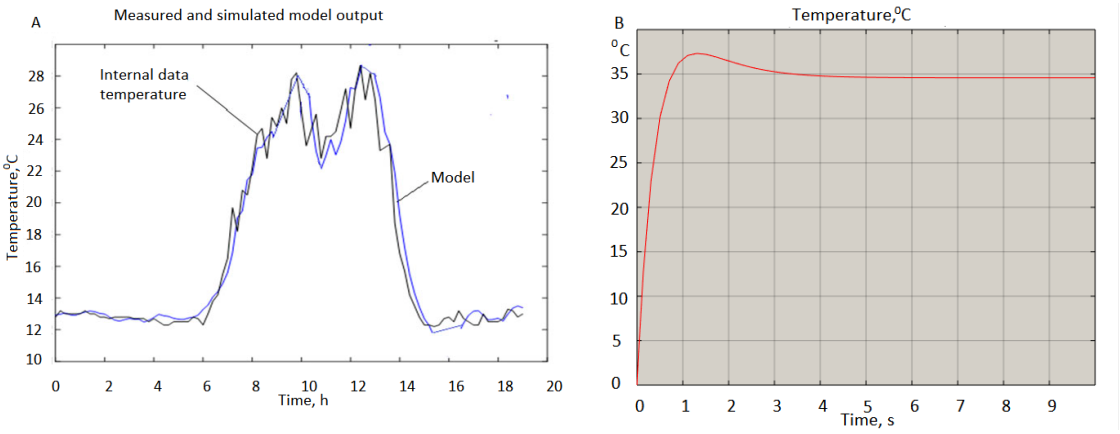


Figure 6. Measured and simulated model output (A) and step response (B). The record shown in panel A spans approximately 19 h; the abscissa of panel B is labelled in seconds.

A further limitation is structural. Equation (4) maps outdoor temperature to indoor temperature, but the dominant forcing of a greenhouse thermal balance is solar radiation, which the model does not contain. The identification's own selection criterion — days of similar radiation and wind — is the admission that radiation was held roughly constant rather than modelled. The model is therefore a black-box surrogate valid over the radiation regime of the identification data, and it should not be extrapolated to different ones.

4.2 Air-exchange time is a ventilation quantity, not a thermal constant

The extractor was sized from the greenhouse volume, 150 m³, and an air-change rate of 28 h⁻¹, which gives the adopted flow rate of 4200 m³/h. Equation (5) states both quantities:

$$\mathrm{ACH} = \frac{Q}{V}, \qquad \tau_{\mathrm{air}} = \frac{V}{Q} \tag{5}$$

Substituting, ACH = 4200/150 = 28 h^{-1} and τ_{air} = 150/4200 h = 2.14 min = 128.6 s. The arithmetic is correct and the sizing is coherent: one complete air renewal every 2.14 min is the order of magnitude convective cooling requires in protected agriculture. The windows, which represent 20 % of the greenhouse area, are operated by two synchronised motors.

What this quantity is not is a thermal time constant. The engineering documentation reports 128.6 s rounded to 128 s as the system time constant and derives from it a stabilisation time of 6 to 11 minutes; three and five times the air-exchange time are 6.43 and 10.71 min, which reproduces that range exactly and identifies its provenance beyond doubt. The figure is V/Q and nothing else: it is the nominal air-exchange time of the ventilation system, the time in which the extractor displaces one greenhouse volume, and it was not obtained from any thermal response estimation. It is renamed accordingly throughout this paper.

The distinction is not terminological. Under either reading of the time unit of equation (4), the identified thermal dynamics and the air-exchange time are different quantities of different magnitude: with the hours reading the dominant thermal constant is 48.5 min against 2.14 min of air exchange, a factor of 22.6; with the seconds reading it is 0.81 s against 128.6 s. A thermal envelope stores energy in the structure, the substrate and the crop, and it does not equilibrate in the time the fan needs to replace the air.

A Simulink simulation of the on-off extractor loop was run with a mean reference of 28 °C, a minimum of 25 °C and a maximum of 31 °C. Figure 7 shows the resulting limit cycle between those two bounds, which is the expected behaviour of an on-off controller with a dead band and confirms that the bounds were implemented as stated. The period of the cycle inherits the time-unit ambiguity of the model: read in seconds as plotted, the extractor would switch about 69 times per hour, which is operationally implausible for the electromechanical installation described and therefore reinforces the need to verify the model time base; read in the corresponding hours scale the same trace gives a period of the order of one hour, which is operationally sensible. The simulation is reported as evidence of the dead-band design and not as a prediction of switching frequency.

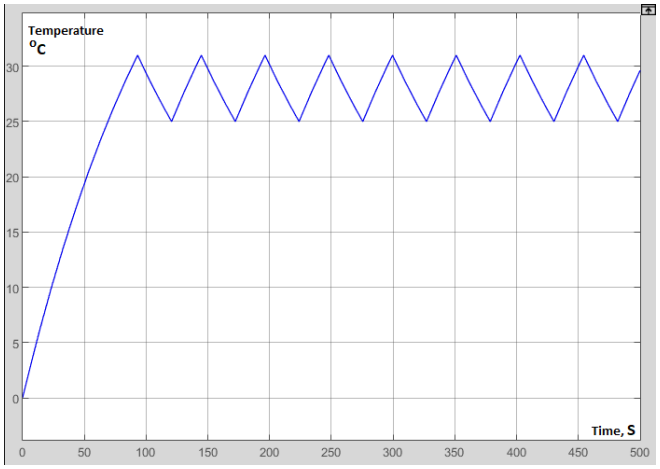


Figure 7. Simulated indoor temperature under on-off control of the extractor for a reference of 28 °C with bounds at 25 and 31 °C.

4.3 Indoor temperature

Table 3 reproduces the average daily temperatures measured without the control system. The indoor temperature reaches values close to 40 °C at midday while the outdoor temperature is 25 °C, and falls to values close to the outdoor one overnight.

Indoor temperature (°C)	Outdoor temperature (°C)	Time (h)
13	12	1:00
13	13	6:00
40	25	11:00
38	24	16:00
14	13	22:00

Table 3. Average daily temperature values measured without the control system.

Figure 8 shows indoor and outdoor temperature with the control system in operation. The plotted indoor maximum is approximately 26 °C against an outdoor maximum of approximately 29 °C, and the indoor series stays below the outdoor one throughout the central hours of the day. The reduction with respect to the uncontrolled condition of Table 3 is substantial, but the two records belong to different days: the uncontrolled day reached 40 °C indoors with 25 °C outdoors, and the controlled day reached about 26 °C indoors with a higher outdoor maximum. The comparison is therefore a before-and-after observation under different external conditions, not a paired experiment, and it is reported as such.

One consistency item is left open. Three series of indoor temperature appear in this paper, and they do not agree on the maximum reached. Figure 8, the only one explicitly recorded with the control system active, peaks at approximately 26 °C. The identification record of Figure 6A peaks at approximately 28.7 °C and the series of Figure 9 at approximately 32 °C, and for neither of the two was it logged whether the control system was operating. The controlled maximum is accordingly reported as approximately 26 °C from Figure 8 alone, and the status of the other two series remains open. The difference between daytime and early-morning behaviour remains the main control challenge, and it follows from the site: an Andean location at 2750 m has a large diurnal range.

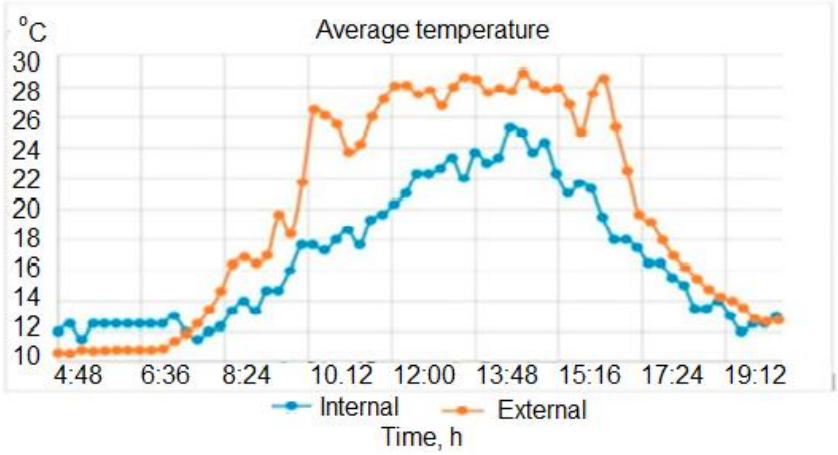


Figure 8. Indoor and outdoor temperature with the control system in operation.

4.4 Substrate moisture

Figure 9 plots the temperature and the average substrate moisture of one day at 20-minute intervals. The moisture series stays between 50 and 80 % with an average of 68 %, which the irrigation loop holds under demanding conditions. The averaging in the legend is across the instrumented rows, which is the natural summary of a per-row quantity.

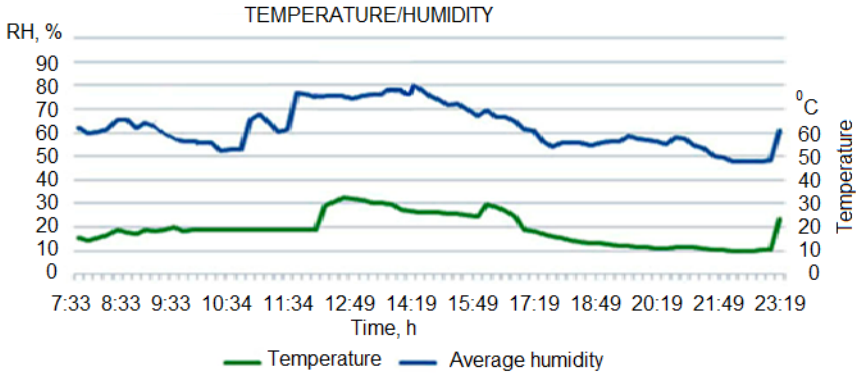


Figure 9. Temperature and average substrate moisture over one day. The percentage series is the average of the FC-28 readings and is a substrate-moisture index on the controller's percentage scale, not an atmospheric relative humidity.

Three statements about this record need to be separated. The moisture band is held, and that is a result of the irrigation loop. The band itself is an experimental controller set point rather than an agronomic optimum: the flowchart of Figure

3 enters a range of 40 to 80 % and the recorded operation lies between 50 and 80 %, and no crop-specific agronomic source establishes an optimal range for the species grown. And the values are readings of a resistive probe adjusted against an HM 445 reference meter reported with ±5 % accuracy — a figure of that reference instrument, not an accuracy of the FC-28 channel, whose calibration curve and measurement uncertainty are not available — with no conversion to volumetric water content documented, so they are reported as a substrate-moisture index on the controller's percentage scale. The behaviour is consistent with the automatic irrigation reported by Sivagami et al. [24], where a soil moisture sensor likewise sets the irrigation times.

For the same reason the temperature band is described as an experimental set point. The range of 26 to 30 °C is not supported by any crop-specific source as a general recommendation; the instrumented cycle grew quinoa, and the values are reported here as the bounds configured in the controller.

4.5 Cycle report

The SCADA system organises access from a main screen to the control functions and to the historical reports. Production reporting requires entering the dates of interest, together with the offline data — fertiliser type and consumption and the number of germinated seedlings — after which the report of Table 4 is obtained.

Field	Value
Operator	Operator A (anonymised)
Identity document	Not published (personal data)
Start date	17/11/2024
End date	10/01/2025
Crop	Quinoa
Initial number of seedlings	300
Number germinated	270
Fertiliser type	Compound 1
Fertiliser used (L)	30
Water used (L)	200
Energy per seedling (kWh/seedling, as recorded)	0.008
Total cost per seedling	0.230
Observation	None

Table 4. Cycle report produced by the SCADA system. The operator's name and identity document have been withheld: they identify a third party who is not an author.

The germination rate of the instrumented cycle is 90.0 % — 270 seedlings of 300 — and it is reported as a descriptive outcome. No baseline or control cycle is available, so no causal attribution of this rate, or of any change in productivity, to the control system is made or can be made from this design.

One field of Table 4 does not reconcile with the rest of the data. The cycle runs from 17 November 2024 to 10 January 2025, that is 54 days, and the measured average load is 7 kWh per day, which gives about 378 kWh over the cycle and about 1.4 kWh per seedling. The tabulated figure of 0.008 kWh per seedling is smaller by a factor of about 175. The field label mixes a currency symbol with an energy unit, so the discrepancy may be a unit error rather than a measurement error, and it is left unresolved here: no interpretation of that field is adopted, and none of the conclusions of this paper depends on it.

4.6 Energy

Two energy questions must be kept apart: how much energy the installation consumed, which the analyser measured, and how much the photovoltaic subsystem supplied, which it did not resolve.

On the first, the Sentron PAC 3200 recorded an average daily consumption of 7 kWh over a measurement period of 7 days. That is a measurement and it is retained.

On the second, the available data do not support an autonomy claim, and the reason is instrumental before it is arithmetical. The SCADA configuration of Figure 2 reports a single energy channel, and the microgrid of Figure 1 places the utility supply behind an automatic transfer system, so the recorded consumption does not separate the fraction served by the photovoltaic subsystem from the fraction taken from the grid. No generation time series, no battery state of charge and no import or export metering are available. What the seven-day window establishes is that

the installation as a whole, photovoltaic subsystem and grid transfer together, covered the recorded load over that window.

The storage figure is likewise undetermined. A capacity in ampere-hours is not an energy: the usable energy of the bank follows equation (6), where V_{nom} is the nominal bus voltage, C the rated capacity, DoD the admissible depth of discharge and η the combined conversion efficiency.

$$E_{\mathrm{usable}} = V_{\mathrm{nom}} \cdot C \cdot \mathrm{DoD} \cdot \eta \tag{6}$$

None of the three factors beyond the capacity is documented. The only voltage that appears in the engineering documentation is the 24 V DC supply of the control cabinet, which is a control-power rail and does not determine the battery bus; the number of cells drawn in Figure 1 is a pictogram and not a wiring diagram. Table 5 shows what the 500 Ah rating implies under the three usual bus voltages, with the depth of discharge and the efficiency set at illustrative values that are stated as assumptions and are not measurements of this installation.

Nominal bus voltage (V)	Nominal energy (kWh)	Usable energy with DoD = 0.5 and η = 0.9 (kWh)	Covers one day of the recorded load?
12	6	2.7	No
24	12	5.4	No
48	24	10.8	Yes

Table 5. Usable storage energy implied by the 500 Ah rating as a function of the nominal bus voltage, against the recorded daily load of 7 kWh. The depth of discharge and the efficiency are declared illustrative assumptions, not measured values of this installation.

The table makes the gap concrete rather than filling it, and the uncertainty is not marginal: with a 12 or 24 V bus the bank would not carry one day of the recorded load, and only a 48 V bus would. Claims of 24 hours of autonomy, of energy autonomy and of energy self-sufficiency therefore cannot be sustained. On the generation side the same arithmetic applies: covering 7 kWh a day from 1.5 kWp requires at least 4.67 equivalent peak sun hours even at a performance ratio of one, and any realistic ratio raises that requirement, so the sizing is not obviously comfortable and no generation record exists to settle it. The claim that surplus energy is delivered to the adjacent laboratory cannot be sustained either, for the same reason and because the topology of Figure 1 shows the laboratory as a parallel load rather than as the recipient of an export.

Energy performance can nevertheless be defined for future use. Following Salazar, Cruz and Rojano [21], equations (7) to (9) give the energy-use efficiency η_{E}, the energy productivity P_{E} and the specific energy e_{s}:

$$\eta_{\mathrm{E}} = \frac{E_{\mathrm{out}}}{E_{\mathrm{in}}} \tag{7}$$

$$P_{\mathrm{E}} = \frac{Y}{E_{\mathrm{in}}} \tag{8}$$

$$e_{\mathrm{s}} = \frac{E_{\mathrm{in}}}{Y} = \frac{1}{P_{\mathrm{E}}} \tag{9}$$

Here E_{in} is the energy input and E_{out} the energy output, both per unit area in MJ·m⁻², so that η_{E} is dimensionless; Y is the greenhouse production per unit area in t·m⁻², so that P_{E} is expressed in t·MJ⁻¹ and e_{s} in MJ·t⁻¹. The last two are reciprocals of each other, which equation (9) states explicitly. Energy productivity measures the efficient use of energy, but a high value does not by itself make an operation economically viable, and the agronomic aspects of the harvest have to be weighed alongside it. None of the three indicators is instantiated here: E_{out} requires an energy content of the harvested product that is not available, and Y is reported as a seedling count rather than as a mass per unit area.

5. DISCUSSION

The platform works. It measures indoor temperature and substrate moisture, closes an irrigation loop on the second and a staged ventilation loop on the first, reports a production cycle through a SCADA system, and runs on a

photovoltaic microgrid with grid backup. Indoor temperature under control stays well below the values recorded without it. That result is solid and supports the installation as an experimental facility.

What this paper contributes is not confirmation but delimitation, and the largest item is a variable identity. A greenhouse has two humidity loops that share a name and share nothing else: the substrate, which belongs to irrigation, and the air, which belongs to climate and is where a misting interlock would act. The installation instruments the first and not the second. Once that is stated, several claims cannot be made — air-humidity control, the misting interlock as deployed logic, and any interpretation of Figure 9 as an atmospheric record — while the irrigation result itself is unaffected and, if anything, becomes easier to read.

The second item is the status of the control formalism. Four modes, three actuators and a fixed escalation order make a finite-state supervisory policy, and that is what Table 2 states. They do not make a hybrid automaton: that object carries continuous dynamics attached to each discrete mode, and estimating them requires the incremental thermal effect of each actuator separately, which needs actuator-state logs that are not available. The distinction is not pedantic, because the mode-wise dynamics are exactly what an optimised policy would be computed from. In supervisory finite-state control, tracking dynamic mode transitions under sensor uncertainty adheres to the principle that internal system verdicts must faithfully track incoming evidence [13]. Furthermore, discriminating between supervisory control regimes and ranking operational states under multi-attribute trade-offs follows established multicriteria selection frameworks for algorithmic architectures [12].

The third is the difference between a quantity that was computed and one that was measured. The air-exchange time follows from the volume and the flow rate by division; the thermal dynamics were identified from temperature data; the usable storage energy was neither computed nor measured, because the factors it needs are absent. Reporting the first as if it were the second was the error, and the corrected version loses nothing: the ventilation sizing remains justified and the identified model remains available.

The limits that remain are of three kinds. Metrologically, no instrument in the installation has a documented range or accuracy — the documented ±5 % belongs to the HM 445 reference meter, not to the FC-28 channel adjusted against it — and the identified model has an in-sample fit and no held-out validation. Experimentally, the controlled and uncontrolled records belong to different days, and the germination rate has no baseline, so no causal attribution is available for either. Energetically, a seven-day consumption record with no generation series and no bus voltage establishes feasibility over that window and nothing beyond it.

6. SCOPE AND FUTURE WORK

The contribution is the instrumented platform, the identified thermal response and the formalisation of the control policy actually deployed. Four extensions follow directly, and each is stated with the measurement it requires, since none of them can be carried out with the present data. Table 6 summarizes the four extensions.

An atmospheric-humidity transmitter with a documented range and accuracy, sited in the greenhouse air and wired to the PLC, would make equation (3) instantiable, would allow the misting interlock to be implemented as a guard the controller can evaluate, and would separate the climate loop from the irrigation loop for good.

Logging actuator states jointly with the climate variables would allow the incremental dynamic effect of each actuator to be estimated — the cooling attributable to natural ventilation, to forced extraction and to misting separately. Those mode-wise dynamics are what the present formalism lacks, and only with them does the supervisory policy become a hybrid automaton in the proper sense.

With those coefficients the escalation policy becomes a finite-horizon optimal control problem with binary actuator decisions, in which the decision at each step minimises the deviation from the crop-specific band together with the energy, water and switching costs, subject to the identified dynamics and to the actuator sequencing constraints. Comparing its solution with the deployed escalation on time in band, integral tracking error, energy, water and number of switches would establish whether the deployed sequence is itself optimal. That comparison is not attempted here: without actuator-state data the optimisation has no model to be solved against, and reporting one would report nothing.

Finally, a seasonal record of photovoltaic generation and load, together with the nominal bus voltage and the battery configuration, would allow the self-sufficiency fraction and the loss-of-load probability to be computed, which is what an autonomy claim requires. A control cycle run alongside an uncontrolled one would supply the baseline that the productivity question needs.

Extension	Measurement required	Expected direction
Separate the climate loop from the irrigation loop; instantiate equation (3); implement the misting interlock	Atmospheric-humidity transmitter (documented range/accuracy) in the greenhouse air, wired to the PLC	Enables a genuine climate loop distinct from irrigation; equation (3) becomes usable; misting interlock becomes evaluable by the controller
Estimate the incremental dynamic effect of each actuator (ventilation, forced extraction, misting)	Logging actuator states jointly with the climate variables	Turns the supervisory policy into a hybrid automaton in the proper sense; separates cooling attributable to each actuator
Test whether the deployed escalation sequence is itself optimal	Actuator-state data feeding the mode-wise dynamics above	Would allow posing the escalation as a finite-horizon optimal control problem and comparing it with the deployed policy on time in band, tracking error, energy, water and switching count
Compute the self-sufficiency fraction and loss-of-load probability; establish a productivity baseline	Seasonal record of PV generation and load, nominal bus voltage, battery configuration; a parallel uncontrolled cycle	Would support or refute an autonomy claim; would give the baseline the productivity question needs

Table 6. The four extensions proposed in Section 6, with the measurement each requires and its expected direction.

6.1 Structural form of the optimal policy, independent of the missing data

Section 6 leaves the optimal control problem unsolved for lack of data; this subsection asks a narrower question that the same formulation already answers without that data — not what the optimal policy is, but what shape it must have.

The finite-horizon problem just stated can be specified without the missing actuator-state data, and the specification already yields a structural result. Let the state be the pair (T_t, m_t), indoor temperature and the currently active mode; let the action a_t be the commanded mode, constrained by the ratchet structure of Section 3.2 to $A(s_t) = \{m_t, \dots, 3\}$ before 18:00 and to $\{0,1,2,3\}$ at the reset. Mode evolves deterministically, $m_{t+1} = a_t$, and temperature evolves as $T_{t+1} = f_{a_t}(T_t, w_t)$ for an exogenous disturbance w_t and a mode-specific response f_a that is exactly the coefficient this section already identified as unavailable. The one-step cost is

$$c(T_t, a_t) = w_T \max(T_t - T_{\text{ref}}, 0)^2 + w_E E(a_t) + w_W W(a_t) + w_S \mathbf{1}[a_t \neq m_t] \tag{10}$$

a weighted sum of temperature deviation above the reference, the energy and water drawn by the active actuators, and a switching penalty — the same four quantities Section 6 already names, with weights w_T, w_E, w_W, w_S left as free parameters that the present data do not fix. The Bellman recursion is

$$V_t(T, m) = \min_{a \in A(T,m)} \{c(T, a) + \mathbb{E}[V_{t+1}(f_a(T, w), a)]\} \tag{11}$$

with V_H a terminal cost.

This problem belongs to the class for which monotone control-limit policies are optimal under standard sufficient conditions — conditions that are stated here as assumptions, not verified, because verifying them needs exactly the mode-wise dynamics and cost weights this section already reports as absent. If the one-step cost is non-decreasing and submodular in (T, a) — escalating is weakly less costly, at the margin, the hotter the state already is — and the transition kernel is stochastically monotone and submodular in (T, a) — a stronger action produces a stochastically cooler next state, and that effect does not shrink as T grows — then a general result for this problem class gives a threshold $T^*(m)$ for each mode m such that escalating past m is optimal exactly when $T \geq T^*(m)$ [20, 26]. The general result allows a different threshold per mode; the deployed policy of Table 2 is the special case in which all four thresholds coincide at the single configured reference, $T^*(m) = T_{\text{ref}}$ for every m. That equality is an additional simplification of the deployed logic, not a consequence the theorem forces, and it is stated here as an observation about Table 2, not as a derived result.

Two things follow from this, and they should not be run together. First, the qualitative shape of the deployed policy — a threshold rule in temperature, escalating and never de-escalating within the horizon — belongs to the class that monotone-control theory identifies as optimal under the two conditions above; it is not the only member of that class, and whether those two conditions actually hold for this greenhouse has not been checked. Second, the single shared threshold the deployed policy uses is a stronger, additional restriction that the cited results do not by themselves justify: a supermodular cost and a monotone transition kernel are compatible with mode-dependent thresholds $T^*(0) < T^*(1) < T^*(2)$ that need not coincide with T_{ref}. Reporting the deployed policy as optimal, or as validated by this argument, would overstate what is shown. What is shown is narrower: the general shape is theoretically motivated under stated, unverified assumptions, and the further simplification to one shared threshold is a property of the deployed logic worth checking, not one this subsection establishes. Closing either gap — verifying the two sufficient conditions, or testing whether a single shared threshold is actually efficient against mode-specific ones — needs the same actuator-state data the extension above already asks for.

7. CONCLUSIONS

An experimental greenhouse of 50 m² was instrumented and operated under automatic control, and the platform performed as an experimental facility: indoor temperature, substrate moisture, irrigation water and electrical consumption are measured, supervised from a SCADA system and reported per production cycle.

The measured climate response is the clearest result. Without control the indoor temperature reached values close to 40 °C at midday against 25 °C outdoors; with control in operation the plotted indoor maximum is approximately 26 °C and the indoor series stays below the outdoor one through the central hours. The two records belong to different days and the comparison is therefore observational.

The humidity result is a substrate-moisture result. The eight FC-28 probes report a substrate-moisture index on the controller's percentage scale for the crop rows — not a volumetric water content, since no calibration curve or conversion is available — the loop they close is irrigation, and the recorded operation holds the band between 50 and 80 % with an average of 68 %. The installation contains no atmospheric-humidity instrument, so no measurement or control of the relative humidity of the greenhouse air is claimed.

The deployed temperature controller is a four-mode finite-state supervisory policy with a fixed escalation order, driven by the persistence of a single temperature condition. Its structure is reproducible; its numerical thresholds were not preserved. It carries neither a release margin nor a humidity interlock, and both are proposed here for a future implementation rather than reported as executed logic. As a four-mode structure driven by a single persistent condition with a fixed escalation order, this policy is not specific to this installation: the same structure is transferable to any greenhouse deployment that escalates a control response from a single sensed condition, independently of the numerical thresholds used here.

The identified model relating outdoor to indoor temperature is retained with an 88 % in-sample fit and no independent validation, and its time unit is not fixed by the available data. The nominal air-exchange time of the ventilation system is V/Q = 128.6 s; it is a ventilation quantity and not an identified thermal constant, and the stabilisation range of 6 to 11 minutes is three to five times that value.

On energy, the analyser recorded an average load of 7 kWh per day over seven days. The measurements do not separate photovoltaic supply from grid import, and the usable energy of the 500 Ah bank is undetermined without the nominal bus voltage, the admissible depth of discharge and the conversion efficiency. No claim of energy autonomy, of 24 hours of autonomy or of surplus export is made.

A germination rate of 90.0 % was recorded in the instrumented cycle. It is a descriptive outcome: with no baseline cycle, no attribution of it to the control system is possible, and the conditions maintained are described as consistent with the experimental control set points rather than as a demonstrated biological effect.

RECEIVED: APRIL, 2026.
REVISED: SEPTEMBER, 2026.

REFERENCES

[1] ALARCÓN, L. A., ARIAS, V. G., DÍAS, O. C. and SOTTO, V. J. (2017): Diseño de un sistema de control y automatización de temperatura, humedad del suelo y humedad relativa para optimizar el rendimiento de cultivos bajo cubierta en Corhuila. **4to Congreso Internacional Amitic 2017**, Popayán, Colombia. https://ridda2.utp.ac.pa/handle/123456789/1686

[2] ALVES, D. F., BARRETO, M. L., YANAGI, J. T., LUIZ, O. J. and OSORIO, S. J. (2017): Evaluación de la eficiencia del enfriamiento evaporativo en invernaderos equipados con placas porosas húmedas. **Dyna**, 84(203), 118-125.

[3] AMANOWICZ, Ł., RATAJCZAK, K. and DUDKIEWICZ, E. (2023): Recent advancements in ventilation systems used to decrease energy consumption in buildings — literature review. **Energies**, 16(4), 1853. https://doi.org/10.3390/en16041853

[4] AMAYA, E. A. (2015): Diseño e implementación de sistema de riego automatizado en un invernadero de la Escuela Nacional de Agricultura, ENA. **Revista Tecnológica**, 7(1), 48-53.

[5] AZAZA, M., TANOUGAST, C., FABRIZIO, E. and MAMI, A. (2016): Smart greenhouse fuzzy logic based control system enhanced with wireless data monitoring. **ISA Transactions**, 61, 297-307. https://doi.org/10.1016/j.isatra.2015.12.006

[6] CASTAÑEDA, R., HERRERA, G. and GARCÍA, E. J. (2003): Modelación física de un invernadero para el desarrollo de un sistema de control climático. **Naturaleza y Desarrollo**, 1(2), 16-24.

[7] FLORES, A., MORALES, A. and PUEBLA, H. (2021): Multivariable control of the greenhouse climate. **Memorias del Congreso Nacional de Control Automático, AMCA, Guanajuato, México**, 208-213. https://revistadigital.amca.mx/wp-content/uploads/2022/06/0073-1.pdf

[8] GONZÁLEZ, I. and CALDERÓN, A. (2009): Automation of greenhouses with programmable controller and decentralized periphery via fieldbus. **IEEE International Conference on Mechatronics**, Málaga, España. https://doi.org/10.1109/ICMECH.2009.4957160

[9] GORTARI, R. R. (2012): Xochimilco como alternativa de competitividad para los orgánicos: el caso de invernaderos Tepexomulco. **Nueva Antropología**, 25(77), 59-78.

[10] GUOXIANG, Z., XINGXING, L., ZETIAN, F., STANKOVSKI, S., YUHONG, D. and XINXING, L. (2019): Mediciones precisas y control de la posición de la persiana enrollable y la película enrollable en un invernadero solar. **Journal of Cleaner Production**, 228, 645-657. https://doi.org/10.1016/j.jclepro.2019.04.129

[11] KABATO, W., GETNET, G. T., SINORE, T., NEMETH, A. and MOLNÁR, Z. (2025): Towards climate-smart agriculture: strategies for sustainable agricultural production, food security, and greenhouse gas reduction. **Agronomy**, 15(3), 565. https://doi.org/10.3390/agronomy15030565

[12] LEYVA VÁZQUEZ, M. Y., BRIONES PEÑAFIEL, L. A., SÁNCHEZ MUÑOZ, S. X. and QUIROZ MARTÍNEZ, M. A. (2021): A framework for selecting machine learning models using TOPSIS. **Advances in Intelligent Systems and Computing**, 1213, 119-126. https://doi.org/10.1007/978-3-030-51328-3_18

[13] LEYVA VÁZQUEZ, M. Y., MATHEU PÉREZ, A. and SMARANDACHE, F. (2026): Internal verdicts track evidence: a template-controlled neutrosophic reading of epistemic states in large language models via the Jacobian lens. **Neutrosophic Sets and Systems**, 101, 1-8. https://doi.org/10.5281/zenodo.22249786

[14] MAHATO, H. M. (2025): Human-centric biotechnological interventions: a pillar for sustainable agricultural development in industrial crop improvement. Springer Nature. https://doi.org/10.1007/978-3-031-75937-6_12

[15] MAMANI, M., VILLALOBOS, M. and HERRERA, R. (2017): Low-cost web system to monitor and control an agricultural greenhouse. Ingeniare. **Revista Chilena de Ingeniería**, 25(4), 599-618. https://doi.org/10.4067/S0718-33052017000400599

[16] MARAVEAS, C., KARAVAS, C.-S., LOUKATOS, D., BARTZANAS, T., ARVANITIS, K. G. and SYMEONAKI, E. (2023): Invernaderos agrícolas: tecnologías de gestión de recursos y perspectivas para cero emisiones de gases de efecto invernadero. **Agriculture**, 13(7), 1464. https://doi.org/10.3390/agriculture13071464

[17] MARRERO, R. S., GUZMÁN, R. D., GONZÁLEZ, P. I., LEÓN, S. M. and LEÓN, S. A. (2021a): Energy efficiency of a greenhouse: a practical study of application of a multifrequency controller in a multivariable environment. **Brazilian Journal of Development**, 7(6), 58234-58249. https://doi.org/10.34117/bjdv7n6-293

[18] MARRERO, R. S., GONZÁLEZ, P. I., LEÓN, S. M. and SUÁREZ, V. R. (2021b): Control de humedad y consumo de agua en un invernadero. **Universidad, Ciencia y Tecnología**, 25(109), 60-70. https://doi.org/10.47460/uct.v25i109.449

[19] MONTERO, J. I., STANGHELLINI, C. and CASTILLA, P. N. (2008): Greenhouse for sustainable production in mild winter climate areas. **Horticulture International**, 65, 14-28.

[20] PUTERMAN, M. L. (1994): **Markov Decision Processes: Discrete Stochastic Dynamic Programming**. Wiley, New York.

[21] SALAZAR, M. R., CRUZ, M. P. and ROJANO, A. A. (2012): Eficiencia en el uso de la energía en invernaderos mexicanos. **Revista Mexicana de Ciencias Agrícolas**, 4, 736-742.

[22] SALAZAR, M. R., MAURICIO, P. A., LÓPEZ, C. I. and ROJANO, A. A. (2016): A model of humidity within a semi-closed greenhouse. **Revista Chapingo Serie Horticultura**, 22(1), 27-43. https://doi.org/10.5154/r.rchsh.2015.06.011

[23] SALAZAR, M. R., LÓPEZ, C. I. and SÁNCHEZ, C. A. (2019): Dynamic energy balance model in a greenhouse with tomato cultivation: simulation, calibration and evaluation. **Revista Chapingo Serie Horticultura**, 24(1), 46-60.

[24] SIVAGAMI, A., HAREESHVARE, U., MAHESHWAR, S. and VENKATACHALAPATHY, K. (2018): Automated irrigation system for greenhouse monitoring. **Journal of The Institution of Engineers: Series A**, 99, 183-191. https://doi.org/10.1007/s40030-018-0264-0

[25] TANGARIFE, H. T., TORO, S. X. and CARMONA, C. V. (2020): Sistemas automatizados para el control del recurso hídrico y variables ambientales bajo invernadero: aplicaciones y tendencias. **Entre Ciencia e Ingeniería**, 14(27), 91-98. https://doi.org/10.31908/19098367.1796

[26] TOPKIS, D. M. (1978): Minimizing a submodular function on a lattice. **Operations Research**, 26(2), 305-321.

[27] TREJO, E. C. and LORENZO, I. L. (2012): Técnicas de inteligencia artificial en modelado y control del ambiente de invernaderos: estado del arte, parte 2. **Ingeniería Agrícola y Biosistemas**, 3(2), 81-86. https://doi.org/10.5154/r.inagbi.2011.11.006

[28] VARGAS, M., PALACIOS, M., HUITZILIHUITL, J., CAMACHO, V., AGUILAR, J. and OCAMPO, G. (2015): Factores de innovación en agricultura protegida en la región de Tulancingo, México. **Revista Mexicana de Ciencias Agrícolas**, 6(4), 827-840.

[29] ZHANG, H., CHEN, L., LIU, K. and DU, S. (2013): The design of greenhouse automatic control system based on RS-485 protocol. **Third International Conference on Instrumentation, Measurement, Computer, Communication and Control**, Shenyang, China, 1693-1696. https://doi.org/10.1109/IMCCC.2013.374